with $\bar{u} = N_h/(a_1^*|q_h|)$, $\bar{v} = N_k/(b_1^*|q_k|)$, $\bar{w} = N_l/(c_1^*/|q_l|)$ ($N_h$, $N_k$, $N_l$ are the numbers of unit cells along the crystal edges parallel to $\mathbf{a}_1$, $\mathbf{b}_1$, $\mathbf{c}_1$), so that the result given by one of us for the cube (see, for example, Wilson, 1949, p. 43, equation 26) is readily converted into equation (1′) of Allegra & Ronca (1979) apart from a factor equal to the unit-cell volume.

Lastly, we shall consider the case of the ellipsoid-shaped crystallite. The line profile of a sphere with radius $\tau$ is given by (Langford & Wilson, 1978)

$$I_{hkl}(s) = N\{\psi^{-2} - \psi^{-3}\sin 2\psi + \tfrac{1}{2}\psi^{-4}(1 - \cos 2\psi)\}, \quad (13)$$

where

$$\psi = 2\pi\tau s, \quad (13')$$

and $N = V_{hk}(0)/U$ is the number of unit cells in the crystal. From the above it readily follows that the diffracted intensity is given by (13) except for the replacement of $N$ with $N_1$ and of $\psi$ with $2\pi R\tau s$, $R$ being given by (11). $p_a$, $p_b$, $p_c$ are here the intercepts of the ellipsoid along three Cartesian axes coinciding with the axes of the unit cell.

### References


ALLEGRA, G., BASSI, I. W. & MEILLE, V. S. (1978). *Acta Cryst.* A**34**, 652–655.

ALLEGRA, G. & RONCA, G. (1978). *Acta Cryst.* A**34**, 1006–1013.

ALLEGRA, G. & RONCA, G. (1979). *Acta Cryst.* A**35**, 1018–1020.

LANGFORD, J. I. & LOUËR, D. (1982). *J. Appl. Cryst.* **15**, 20–26.

LANGFORD, J. I., LOUËR, D. & WILSON, A. J. C. (1980). Proceedings of the Xth Conference on Applied Crystallography, Kozubnik, pp. 176–181.

LANGFORD, J. I. & WILSON, A. J. C. (1978). *J. Appl. Cryst.* **11**, 102–113.

LOUËR, D., VARGAS, R. & LANGFORD, J. I. (1981). *Acta Cryst.* A**37**, C285.

PATTERSON, A. L. (1939). *Phys. Rev.* **56**, 972–982.

WILSON, A. J. C. (1949). *X-ray Optics*. London: Methuen.


*Acta Cryst.* (1983). A**39**, 282–286

# A Technique for the Calculation of Multislice Transmission Functions for Crystals with Large (or Infinite) Repeat Distances in the Beam Direction


BY A. R. WILSON

*Electron Microscope Unit, The University of Sydney, NSW* 2006, *Australia*


(*Received* 1 *September* 1982; *accepted* 25 *November* 1982)


## Abstract

A partially analytic technique for the calculation of electron transmission functions used in multislice calculations is developed. This development utilizes the fact that atomic scattering amplitudes are generally available as fitting parameters to four Gaussians. The result is especially applicable to calculations with a large or infinite repeat distance in the incident-beam direction and initial test calculations give a time saving of a factor of four. Sample results are given for the calculation of images from an inclined stacking fault in gold.


## Introduction

The multislice method (Cowley & Moodie, 1957; Goodman & Moodie, 1974) for the calculation of dynamical electron scattering has been discussed and used extensively (*e.g.* Bursill & Wilson, 1977; Lynch, 1971).

The object is considered as a series of thin slices with the electron wave function at the exit surface of the $n$th slice being given by

$$\psi_n(\mathbf{x}) = [\psi_{n-1}(\mathbf{x}) * p_n(\mathbf{x})]\, q_n(\mathbf{x}), \quad (1)$$

where $q_n(\mathbf{x})$ is the transmission function of the $n$th slice and $p_n(\mathbf{x})$ is the propagation function from the $(n-1)$th to $n$th slice and $*$ represents the convolution integral. In a typical calculation the distance between slices is chosen to be constant and hence all $p_n(\mathbf{x})$'s are the same and need only be evaluated once and then stored in computer memory.

The transmission function is determined by

$$q_n(x,y: z_n,\Delta z) = \exp\{-i\sigma\varphi(x,y: z_n,\Delta z)\} \quad (2)$$

(Cowley & Moodie, 1957), where $\sigma$ is the relativistic interaction constant for electrons and $\varphi(x,y: z_n,\Delta z)$ is the projected potential on the $x,y$ plane due to the crystal potential over the thickness $\Delta z$ from $z = z_n$ to $z_n + \Delta z$. This may be evaluated from the atomic

0567-7394/83/030282-05$01.50 

scattering amplitude, $f_i$, for each atom, $i$, by the relation

$$\varphi_i(x,y: z_n,\Delta z) = \int_{z_n}^{z_n+\Delta z} \mathscr{F}_{u,v,w}\{f_i(u,v,w)\}\,\mathrm{d}z, \qquad (3)$$

where $\mathscr{F}_{u,v,w}$ is the Fourier-transform integral over the reciprocal-space coordinates $u,v,w$ and the constant $h^2/2\pi m_0 e$, where $h$ is Planck's constant, $m_0$ is the rest mass of the electron and $e$ is the electronic charge, has been included in the $f_i$'s. For a periodic crystal the Fourier integrals become discrete summations giving

$$\varphi(x,y: z_n,\Delta z) = \int_{z_n}^{z_n+\Delta z} \sum_{i}^{\text{atoms}} \sum_{hkl} \frac{f_i(h,k,l)}{\Omega} \times \exp\left\{2\pi i\ (x-x_i)\frac{h}{a} + (y-y_i)\frac{k}{b} + (z-z_i)\frac{l}{c}\right\}\,\mathrm{d}z, \qquad (4)$$

where $h$, $k$ and $l$ are integers, $(x_i,y_i,z_i)$ are the coordinates of the $i$th atom in the unit cell, $a,b,c$ are the unit-cell dimensions and $\Omega$ is the unit-cell volume. It can easily be shown that for projection over a whole unit cell (4) becomes

$$\varphi(x,y: 0,c) = c \sum_{i}^{\text{atoms}} \sum_{hk} \frac{f_i(h,k,0)}{\Omega} \times \exp\left\{2\pi i\left[(x-x_i)\frac{h}{a} + (y-y_i)\frac{k}{b}\right]\right\} \qquad (5)$$

and hence (2) may be calculated once and the result stored in a two-dimensional array.

Projection of the whole unit cell gives sufficiently accurate results for small values of $c$ (~2 Å). For larger $c$ (<10 Å) the potential may still be formed over the whole unit cell and then it is considered as occurring on planes with ~2 Å spacing [with a suitable fractional weight, for example, $c$ = 5 Å, say, use (5) to give $\varphi_c$ and then use $\varphi_c \times \frac{2}{5}$ in (2) with a propagation distance of 2 Å for $p$ in (1)]. This is necessary in order to reduce errors introduced by large propagation distances. However, for larger values of $c$ and heavy atoms (see *e.g.* Lynch, 1971) the summation over $l$ in (4) must be performed for each slice with $\Delta z \sim 2$ Å and, if $l$ must be summed over a large range, this will be costly in terms of both computer time and memory. The following section details a technique in which the summation over $l$ and integration over $z$ in (4) are partly determined analytically.

### Partial analytic evaluation of the transmission function

This technique uses the fact that the atomic scattering amplitudes, $f_i$, are commonly tabulated as the fitting parameters of four Gaussians, *viz*:

$$f_i(h,k,l) = \sum_{j=1}^{4} {}^{i}a_j \exp\left\{-{}^{i}b_j\left[\left(\frac{h}{a}\right)^2 + \left(\frac{k}{b}\right)^2 - \frac{2hk}{ab}\cos^2\theta + \left(\frac{l}{c}\right)^2\right]\right\}, \qquad (6)$$

where ${}^{i}a_j$ and ${}^{i}b_j$ are Gaussian fitting parameters, $\theta$ is the angle between the $h$ and $k$ axes and $l$ is assumed (without loss of generality) to be along the direction of propagation perpendicular to the $h,k$ axes. Substitution into (4) and separating out the terms containing $l$ gives

$$\varphi(x,y: z_n,\Delta z) = \sum_{j=1}^{4} \int_{z_n}^{z_n+\Delta z} \sum_{i}^{\text{atoms}} \sum_{hkl} \frac{{}^{i}R_j(h,k,0)}{\Omega} \times \exp\left\{2\pi i\left[(x-x_i)\frac{h}{a} + (y-y_i)\frac{k}{b}\right]\right\} \exp\left\{-{}^{i}b_j\left(\frac{l}{c}\right)^2\right\} \times \exp\left\{2\pi i(z-z_i)\frac{l}{c}\right\}\mathrm{d}z, \qquad (7)$$

where

$${}^{i}R_j(h,k,0) = {}^{i}a_j \exp\left\{-{}^{i}b_j\left(\frac{h^2}{a^2} + \frac{k^2}{b^2}\right)\right\}.$$

When the integration over $z$ is performed, the terms in $l$ become

$$\sum_{l} \exp\left\{-{}^{i}b_j\left(\frac{l}{c}\right)^2\right\} \frac{c}{2\pi i l}\left(\exp\frac{2l\pi i\Delta z}{c} - 1\right) \times \exp\left\{2\pi i(z_n - z_i)\frac{l}{c}\right\} = \sum_{l} \exp\left\{-{}^{i}b_j\left(\frac{l}{c}\right)^2\right\} \frac{c}{\pi l} \sin\frac{\pi l\Delta z}{c} \exp\frac{i\pi l\Delta z}{c} \times \exp\frac{-2\pi i z_i l}{c} \exp\frac{2\pi i z_n l}{c}. \qquad (8)$$

Equation (8) may be considered as a Fourier transform with respect to $w$ (where $w = l/c$ is now a continuous variable and the summation goes to an integration) to give a result in $z_n$. Thus, by the convolution theorem, (8) becomes

$$c\mathscr{F}_w\{\exp -{}^{i}b_j w^2\} * \mathscr{F}_w\left\{\frac{1}{\pi w}\sin \pi\Delta z w\right\} * \mathscr{F}_w\{\exp \pi i\Delta z w\} * \mathscr{F}_w\{\exp -2\pi i z_i w\}, \qquad (9)$$

which gives

$$c\{(\pi/{}^{i}b_j)^{1/2}\exp -z_n^2\pi^2/{}^{i}b_j\} * \begin{Bmatrix}1 & |z_n| < \Delta z/2\\ 0 & |z_n| > \Delta z/2\end{Bmatrix}$$
$$* \delta(z_n + \Delta z/2) * \delta(z_n - z_l)$$
$$= c\int_{z_l-\Delta z}^{z_l} (\pi/{}^{i}b_j)^{1/2}\exp[-\pi^2(z_n-g)^2/{}^{i}b_j]\,dg$$
$$= \frac{c}{\pi^{1/2}}\int_{\pi(z_n-z_l+\Delta z)/{}^{i}b_j^{1/2}}^{\pi(z_n-z_l)/{}^{i}b_j^{1/2}} \exp -p^2\,dp, \qquad (10)$$

which has the form of the error function, $\mathrm{erf}(x)$, and gives

$$\frac{c}{2}\{\mathrm{erf}[\pi(z_n + \Delta z - z_i)/{}^{i}b_j^{1/2}] - \mathrm{erf}[\pi(z_n - z_i)/{}^{i}b_j^{1/2}]\}. \qquad (11)$$

Substitution into (7) shows that the result is the same as for projection over the whole unit cell [(5)] but with each ${}^{i}a_j$ Gaussian fitting term weighted by $1/c$ times the term in (11).

Computation of $q(x)$ using this technique will (as will be seen more clearly in the following section) require summation over atoms outside the slice in which the projected potential is being formed. This replaces the full three-dimensional Fourier transform required previously and will in general be faster and more memory efficient since (*a*) the sum over $l$ in (4) is the same as an out-of-slice atom sum and will have at least the same range as the technique above and (*b*) $f_i(h,k,l)$ will have to be either calculated each time or stored in memory for each atom type, whereas the new technique will only require the calculation and storage of the four parts of $f_i(h,k,0)$ corresponding to each ${}^{i}a_j$ parameter [$j = 1$ to 4, (6)]. The new technique would be expected to show significant savings for large values (or virtually infinite values – amorphous objects, sloping defects) of $c$.

### Alternative derivation in real space

The same result may be derived in real space and gives a clearer indication of the significance of out-of-slice atoms. Equation (6) may be expressed in real space as

$$\sum_{j=1}^{4} {}^{i}a_j(\pi/{}^{i}b_j)^{1/2}\exp\{-(d_i^2 + z_i^2)\,\pi^2/{}^{i}b_j\}, \qquad (12)$$

where $d_i^2$ is the distance to the $i$th atom in the $x,y$ plane. This is just the potential distribution of the $i$th atom and hence the value of the integral of (12) over $z = z_n$ to $z_n + \Delta z$ divided by the value of the integral from $-\infty$ to $+\infty$ will give the fraction of the potential that is in the slice $z_n$ to $z_n + \Delta z$. Now,

$$\int_0^z \exp -p^2\pi^2/{}^{i}b_j\,dp = \text{constant} \times \mathrm{erf}\{\pi z/{}^{i}b_j^{1/2}\} \qquad (13)$$

and $\mathrm{erf}(\infty) = 1$, hence the ratio of the two integrals is

$$\tfrac{1}{2}\{\mathrm{erf}[\pi(z_n + \Delta z - zi)/{}^{i}b_j^{1/2}] - \mathrm{erf}[\pi(z_n - z_i)/{}^{i}b_j^{1/2}]\}, \qquad (14)$$

which is exactly the same as (11) (except for a factor of $c$). Equation (14) is the fractional potential of an atom in the slice and hence is the weight that must be applied to each ${}^{i}a_j$ in the evaluation of $f_i(h,k,0)$ in (5). This is the same result as before and clearly shows that atoms out of the slice must be included until the terms in (14) become small. This may be checked prior to calculation by evaluation of (14) and it would be expected that distances of under 10 Å would be sufficient since atomic potentials are fairly localized and this is the order of value of $c$ at which upper-layer-line effects become important in multislice calculations.

### Practical application

The final prompt for the derivation of the above technique was given by the need to do full $n$-beam multislice calculations for defects – specifically, inclined stacking faults in f.c.c. materials. In general there is no repeat distance in the direction of the transmitted beam. This is specially the case for weak-beam studies where the crystal is tilted, say, 1–4° off a zone orientation so that even the perfect-crystal regions on each side of a stacking fault may not have a true repeat in the beam direction.

If the thickness $\Delta z = c' \sin\theta$ (where $c'$ is the perfect-crystal repeat along the stacking-fault direction) then the successive slices are related to each other by a simple sideways shift equal to $c' \cos\theta$ (see Fig. 1) and

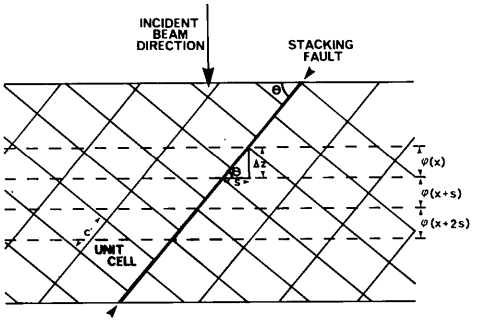


Fig. 1. Schematic diagram of an inclined stacking fault showing lack of periodicity in the beam direction. The shaded areas indicate unit cells on each side of the stacking fault, and slices for which the potentials, $\varphi$, are related by a simple shift are shown by the dashed lines. For f.c.c. structures the unit cell shown is for a [$\bar{1}2\bar{1}$] projection and the stacking fault occurs on (111) planes.

hence only one transmission function need be calculated and then progressively shifted sideways as a phase change in reciprocal space (similar to Lynch, 1971). Figs. 2(*a*) and (*b*) show two different methods for obtaining the same result. The first method involves shifting the transmission function for successive slices whilst the second method shifts the wavefunction. This second method is preferable in the programs used since (1) can be recast to

$$\Psi_n(\mathbf{u}) = \mathscr{F}^{-1}\{\mathscr{F}[\Psi_{n-1}(\mathbf{u})\,P_n(\mathbf{u})]\,q_n(x)\}, \qquad (15)$$

where $\Psi$ and $P$ are Fourier transforms of $\psi$ and $p$ respectively, giving superior calculation times when fast Fourier transforms are used (Self, 1979; MacLagan, 1975). Hence the sideways shift in $\psi(\mathbf{x})$ may be easily included as a phase factor in $P_n(\mathbf{u})$.

## Calculation results

Fig. 3 shows the cell used to test the computer programs and theory. Calculations were performed using (*a*) three transmission functions corresponding to slices 1, 2 and 3 (all 3·13 Å thick), (*b*) one transmission function (slice 1) and a sideways shift of 9·97/9 Å, and (*c*) the same as (*b*) but using the theory included in this paper to include out-of-slice atoms. The

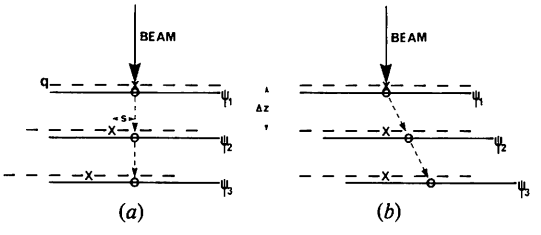


Fig. 2. Progression of the calculation through three successive slices. Dashed lines represent the transmission function, $q$, full lines represent the wavefunction, $\psi$, after each slice and the dashed arrows represent propagation between slices. In (*a*) the transmission function is shifted sideways whilst in (*b*) the same result is obtained with a tilted propagator.

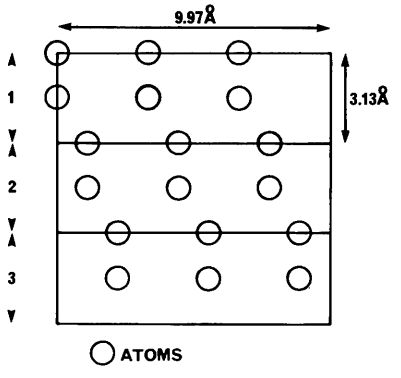


Fig. 3. Test cells used. Cell 2 is related to cell 1 by a $\frac{1}{3}$ *a*-axis (1·108 Å) shift.

results in all cases were essentially identical and indicated that case (*c*) was approximately four times faster than case (*b*) for the calculation of the transmission function. In case (*b*) $f_l(h,k,l)$ was recalculated for each $l$ value in order to simulate a defect calculation where computer memory might be at a premium. A point of interest arose in that it was found necessary to input the atomic positions as accurately as possible to give acceptably low values for the calculated non-Bragg points which should be equal to zero. Thus on a Cyber 170-730 atomic positions were entered as two numbers representing a fraction so that the full precision available was utilized.

As an example of the technique weak-beam images from the 202 beam, $s = -0{\cdot}04$, for gold with a stacking fault on the (111) plane and imaged close to the [010] projection were calculated. Scattering factors due to Doyle & Turner (1967) were used with a periodically continued supercell (MacLagan, Bursill & Spargo, 1977; Wilson, Bursill & Spargo, 1978/79) formed for a single slice satisfying the condition $\Delta z = c' \sin\theta$ (where $c'$ is the gold repeat in the $[\bar{1}2\bar{1}]$ direction, see Fig. 1) with the stacking-fault edge half-way along the supercell. The technique is especially suited to this sort of calculation since there are a large number of atoms in the supercell. Fig. 4 shows schematically how the crystal 'builds up' with thickness. For the supercell-size used it is clear that above 679 Å crystal thickness the scattering from the stacking fault and 'returning defect' at the end of the crystal (inherent in the method of periodic continuation) will overlap. (In fact, in order to avoid overlap of the images the maximum thickness would be restricted to around 620 Å.) Table 1 shows actual and estimated times and costs for the calculation of a 540 Å thick crystal on the Cyber 170-730 at Sydney University. The results for the smallest calculation are presented below and this is

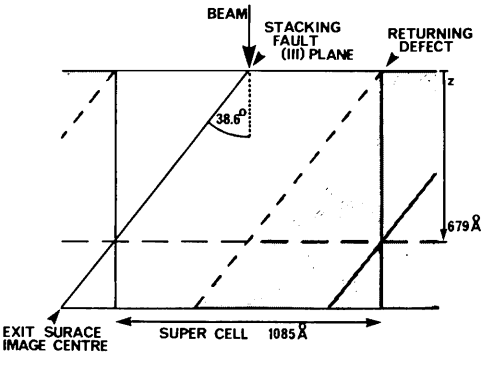


Fig. 4. Schematic diagram of the bulk crystal with a supercell of 1085 Å and a stacking fault inclined at 38·6° to the incident beam. The shaded areas represent the periodically repeating supercells. For thickness, $z$, greater than 679 Å, the scattering from the stacking fault and returning defect at the ends of the supercell will overlap. Note that the intersection of the stacking fault with the exit surface of the crystal will always be in the centre of the calculated image.

Table 1. *Actual (starred column) and estimated CPU calculation times and total job cost for the Cyber 170-730 at Sydney University for increasing number of beams [in terms of the (202) distance] in reciprocal space and a 540 Å thick crystal*

| | (202) distances in reciprocal space | | |
|---|---|---|---|
| | 1·4* | 2·7 | 5·4 |
| Set up transmission function (min.) | 14 | 31 | 69 |
| Perform iteration (min) | 4 | 10 | 22 |
| Cost (dollars) | 45 | 100 | 220 |

thought to be adequate for an initial test because (*a*) the multislice calculation allows for scattering out to twice the number of beams in the calculation [2·8 (202) distances] but not back into the calculation from 1·4 to 2·8 (202) distances, (*b*) the crystal is tilted 3–4° off a zone axis, (*c*) the image is formed from a weakly excited beam, and (*d*) calculations for thinner crystals and twice the number of beams gave the same image results. Various internal checks on the accuracy of the calculations [*e.g.* unitarity test, Moodie (1965); Bursill & Wilson (1977)] indicated that the calculations would be reasonably accurate. Figs. 5 and 6 present examples of calculated stacking-fault images for various values of thickness and defocus. These are only preliminary calculations and will be discussed more fully elsewhere. A brief discussion follows.

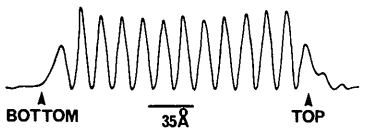


Fig. 5. Weak-beam stacking-fault image profile for $\Delta f = -10\,000$ Å, $C_s = 2{\cdot}5$ mm and 265 Å thick gold using the 202 beam with $s = -0{\cdot}04$ Å$^{-1}$ and an aperture of radius $\frac{1}{4}$ Å$^{-1}$. The fringe spacing is approximately 16·9 Å. 'Top' and 'bottom' indicate the point at which the stacking fault intersects the top and bottom surfaces of the crystal respectively.

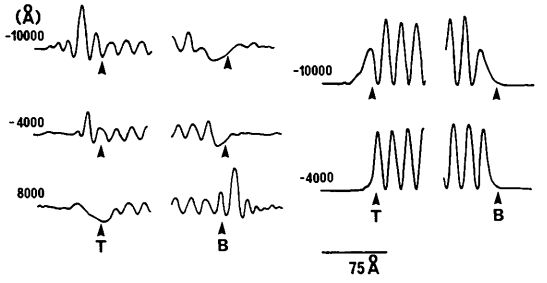


Fig. 6. Weak-beam stacking-fault image profile for defocus values as shown, $C_s = 2{\cdot}5$ mm and (*a*) 538 Å, (*b*) 304 Å thick gold obtained using the 202 beam with $s = -0{\cdot}04$ Å$^{-1}$ and an aperture of radius $\frac{1}{4}$ Å$^{-1}$. Again, the fringe spacing is 16·9 Å and *T* and *B* refer to the intersection of the stacking fault with the top and bottom surfaces of the crystal respectively. The fringe detail between these two points has not been shown since it is a simple continuation of the oscillatory nature close to the stacking-fault ends.

In both figures the oscillating fringes between the intersection of the stacking fault with the top and bottom surfaces of the crystal are fairly simple and have a period of approximately 16·9 Å. This is similar to results obtained for column- and non-column-approximation types of calculations (*e.g.* Jap & Shennin, 1981). The present calculations show that the image may extend past the ends of the stacking fault. This is especially the case for the 538 Å thick calculation where the intensity of the internal fringes is depressed compared with the thinner calculations, with a large bright fringe external to the stacking fault occurring at the top, for overfocus, and bottom, for underfocus, edges of the stacking fault.

I would like to thank Dr D. J. H. Cockayne for giving me the opportunity of working with him at the Electron Microscope Unit, The University of Sydney. The financial support of the Australian Research Grants Scheme is also gratefully acknowledged.

## References

BURSILL, L. A. & WILSON, A. R. (1977). *Acta Cryst.* A**33**, 672–676.
COWLEY, J. M. & MOODIE, A. F. (1957). *Acta Cryst.* **10**, 609–619.
DOYLE, P. A. & TURNER, P. S. (1967). *Acta Cryst.* A**24**, 390–397.
GOODMAN, P. & MOODIE, A. F. (1974). *Acta Cryst.* A**30**, 280–290.
JAP, B. K. & SHEININ, S. S. (1981). *Phys. Status Solidi B*, **105**, 137–145.
LYNCH, D. F. (1971). *Acta Cryst.* A**27**, 399–407.
MACLAGAN, D. S. (1975). MSc Thesis. School of Physics, Univ. of Melbourne.
MACLAGAN, D. S., BURSILL, L. A. & SPARGO, A. E. C. (1977). *Philos Mag.* **35**, 757–780.
MOODIE, A. F. (1965). Int. Conf. on Electron Diffraction and Crystal Defects, Melbourne, ID-1.
SELF, P. G. (1979). PhD Thesis. School of Physics, Univ. of Melbourne.
WILSON, A. R., BURSILL, L. A. & SPARGO, A. E. C. (1978/79). *Optik (Stuttgart)*, **52**, 313–336.